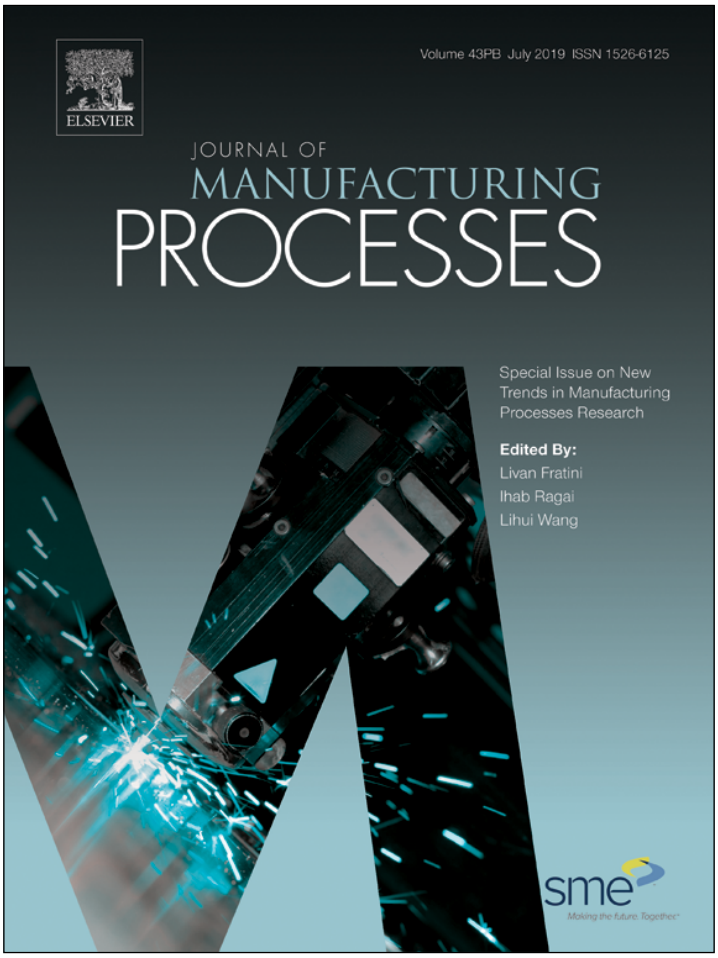

Journal of Manufacturing Processes 43 (2019) 2–11

Contents lists available at ScienceDirect

Journal of Manufacturing Processes

journal homepage: www.elsevier.com/locate/manpro

Multi-point coupling for tool point receptance prediction☆

Tony Schmitz*, Andrew Honeycutt, Michael Gomez, Michael Stokes, Emma Betters

University of North Carolina at Charlotte, Mechanical Engineering and Engineering Science, Charlotte, NC, 28223, USA

ARTICLE INFO

Keywords:
Milling
Dynamics
Receptance coupling substructure analysis

ABSTRACT

This paper describes a multi-point receptance coupling substructure analysis (RCSA) technique for tool point receptance prediction. The portion of the tool inside the holder is coupled to the portion of the holder that clamps the tool at multiple points along the insertion length. The coupling can be rigid or flexible-damped. The procedure is described analytically and then experimental results are presented. The tool point receptances, or frequency response functions, for four carbide tool blank diameters are tested at multiple extension lengths and compared to predictions for an ER32 collet connection. Stiffness matrices are identified for each of the tool blank diameters and reported. Given the predicted tool point receptances, milling process models can be used to select optimized operating parameters at the process planning stage.

Introduction

In milling, an important consideration is the vibration behavior of the cutting tool during material removal. This behavior, which can be stable (i.e., exhibits forced vibration only) or unstable (i.e., exhibits either self-excited or period-*n* bifurcations), depends on the workpiece material, the machining parameters, and the structural dynamics [1]. The workpiece material-tool combination defines the relationship between the commanded chip geometry and the cutting force required to shear away the chip. This relationship is parameterized in the form of a (typically) mechanistic cutting force model and the coefficients for this model can be tabulated. The machining parameters are selected by the user to obtain the desired process performance. The structural dynamics, however, pose a significant challenge because the tool point receptance (also referred to as the frequency response function, or FRF) depends on the machine, spindle, holder, and tool. Further, for end mills clamped in a holder (with a deformable collet or thermal shrink fit connection, for example), the receptance changes with the tool's extension length from the holder.

Because the tool point receptance is required to select stable machining parameters, identifying it for arbitrary tool-holder-spindle-machine combinations is a priority. To reduce the significant time and effort associated with measuring every possible combination, Schmitz first presented the application of receptance coupling substructure analysis (RCSA) to tool point FRF prediction in 2000 [2]. The RCSA technique couples modeled receptances of tools and holders to measurements of the spindle-machine receptances to predict tool point receptances. The ability to predict the tool point receptances (rather than measure each combination) enables the realistic shop floor application of machining process models to optimal machining parameter selection. Since the first RCSA demonstration, many authors have implemented and improved the modeling capabilities for both macro- and micro-scale milling, as well as other applications [3–117].

The purpose of this paper is to continue the RCSA evolution by describing and validating a multi-point coupling approach between the internal tool and external holder in end mill assemblies. The intent is to improve on the single point approach where the end of the extended portion of the tool is coupled to the end of the portion of the tool inside the holder at a single coordinate. The paper proceeds as follows. In section 2, the single point (end-to-end) RCSA procedure is summarized. In section 3, the multi-point approach is described. In section 4, the experimental setup is detailed. In section 5, experimental results are presented where the coupling stiffness and damping values are determined and presented for a range of tool diameters and extension lengths using the multi-point coupling model. Finally, conclusions are provided in section 6.

Single point RCSA

Bishop and Johnson presented closed-form receptances for the analysis of flexural vibrations of uniform Euler-Bernoulli beams with free, fixed, sliding, and pinned boundary conditions [118]. For example, the direct receptances for the free-free beam shown in Fig. 1 due to externally applied harmonic forces $f_1(t)$ and $f_2(t)$, applied at

☆ 47th SME North American Manufacturing Research Conference, NAMRC 47, Pennsylvania, USA.

* Corresponding author.
E-mail address: tony.schmitz@uncc.edu (T. Schmitz).

https://doi.org/10.1016/j.jmapro.2019.03.043
Received 29 October 2018; Received in revised form 23 January 2019; Accepted 8 March 2019
Available online 06 May 2019

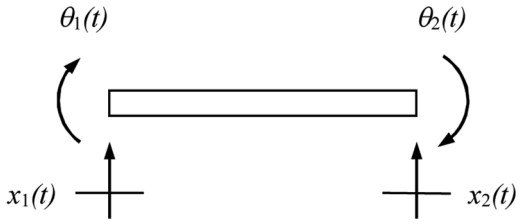

Fig. 1. Free-free beam coordinates.

coordinates $x_1(t)$ and $x_2(t)$, respectively, and moments $m_1(t)$ and $m_2(t)$, applied at $\theta_1(t)$ and $\theta_2(t)$, respectively, are provided in Eq. (1). The corresponding cross receptances are shown in Eq. (2).

$$\begin{aligned} x_1 &= h_{11}f_1 \quad x_1 = l_{11}m_1 \quad x_2 = h_{22}f_2 \quad x_2 = l_{22}m_2 \\ \theta_1 &= n_{11}f_1 \quad \theta_1 = p_{11}m_1 \quad \theta_2 = n_{22}f_2 \quad \theta_2 = p_{22}m_2 \end{aligned} \tag{1}$$

$$\begin{aligned} x_1 &= h_{12}f_2 \quad x_1 = l_{12}m_2 \quad x_2 = h_{21}f_1 \quad x_2 = l_{21}m_1 \\ \theta_1 &= n_{12}f_2 \quad \theta_1 = p_{12}m_2 \quad \theta_2 = n_{21}f_1 \quad \theta_2 = p_{21}m_1 \end{aligned} \tag{2}$$

Eqs. (1) and (2) can be written in matrix form and compactly represented using the notation shown in Eq. (3).

$$\begin{aligned} \begin{Bmatrix} x_1 \\ \theta_1 \end{Bmatrix} &= \begin{bmatrix} h_{11} & l_{11} \\ n_{11} & p_{11} \end{bmatrix} \begin{Bmatrix} f_1 \\ m_1 \end{Bmatrix} \text{or} \{u_1\} = [R_{11}]\{q_1\} \\ \begin{Bmatrix} x_2 \\ \theta_2 \end{Bmatrix} &= \begin{bmatrix} h_{22} & l_{22} \\ n_{22} & p_{22} \end{bmatrix} \begin{Bmatrix} f_2 \\ m_2 \end{Bmatrix} \text{or} \{u_2\} = [R_{22}]\{q_2\} \end{aligned} \tag{3}$$

In Eq. (3), R_{ij} is the generalized receptance matrix that describes both translational and rotational component behavior. The individual entries in these matrices depend on the boundary conditions and include contributions from both the rigid body (if applicable) and flexural modes. For example, at the left end of the free-free beam in Fig. 1, the R_{11} matrix terms are defined by Eq. (4).

$$\begin{aligned} h_{11}(\omega) &= \frac{x_1}{f_1} = \frac{-(\cos\lambda L \sinh\lambda L - \sin\lambda L \cosh\lambda L)}{EI(1+i\eta)\lambda^3(\cos\lambda L \cosh\lambda L - 1)} \\ l_{11}(\omega) &= \frac{x_1}{m_1} = \frac{-(\sin\lambda L \sinh\lambda L)}{EI(1+i\eta)\lambda^2(\cos\lambda L \cosh\lambda L - 1)} \\ n_{11}(\omega) &= \frac{\theta_1}{f_1} = \frac{-(\sin\lambda L \sinh\lambda L)}{EI(1+i\eta)\lambda^2(\cos\lambda L \cosh\lambda L - 1)} \\ p_{11}(\omega) &= \frac{\theta_1}{m_1} = \frac{(\cos\lambda L \sinh\lambda L + \sin\lambda L \cosh\lambda L)}{EI(1+i\eta)\lambda(\cos\lambda L \cosh\lambda L - 1)} \end{aligned} \tag{4}$$

In these equations, the expression for λ is provided in Eq. (5), m is the beam mass (kg), ω is the excitation frequency (rad/s), L is the beam length (m), E is the elastic modulus (N/m^2), I is the second moment of area (m^4), and η is the solid damping factor (unitless) [1].

$$\lambda = \left(\frac{m\omega^2}{LEI(1+i\eta)}\right)^{\frac{1}{4}} \tag{5}$$

These receptances can be used to couple components at their end points in order to predict assembly dynamics. For example, a free-free beam with diameter d_1 can be coupled to a second free-free beam with larger diameter d_2 to synthesize the receptances for a stepped shaft (see Fig. 2). The assembly flexural receptances, shown in Eq. (6) (the upper case variables denote assembly coordinates, forces, moments, and receptances), are determined by first writing the component displacements/rotations; see Eq. (7).

$$\begin{aligned} \begin{Bmatrix} U_1 \\ U_2 \\ U_3 \end{Bmatrix} &= \begin{bmatrix} G_{11} & G_{12} & G_{13} \\ G_{21} & G_{22} & G_{23} \\ G_{31} & G_{32} & G_{33} \end{bmatrix} \begin{Bmatrix} Q_1 \\ Q_2 \\ Q_3 \end{Bmatrix} \text{where} U_i = \begin{Bmatrix} X_i \\ \Theta_i \end{Bmatrix} \\ G_{ij} &= \begin{bmatrix} H_{ij} & L_{ij} \\ N_{ij} & P_{ij} \end{bmatrix} \begin{Bmatrix} f_2 \\ m_2 \end{Bmatrix}, \text{and} Q_i = \begin{Bmatrix} F_i \\ M_i \end{Bmatrix} \end{aligned} \tag{6}$$

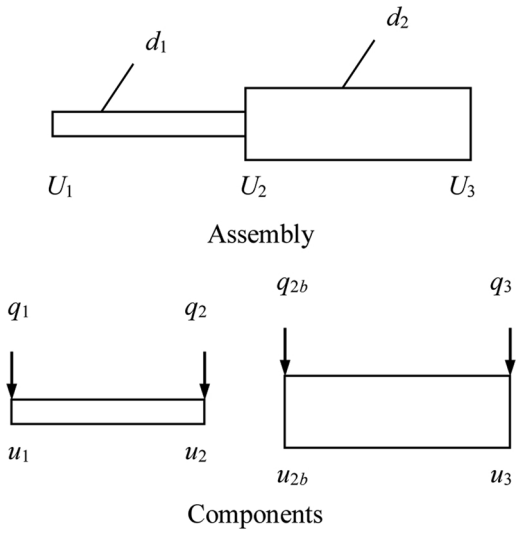

Fig. 2. Stepped shaft assembly (top) and components (bottom). Diameters d_1 and d_2 are identified in the assembly schematic.

$$\begin{aligned} u_1 &= R_{11}q_1 + R_{12}q_2 \qquad u_2 = R_{21}q_1 + R_{22}q_2 \\ u_{2b} &= R_{2b2b}q_{2b} + R_{2b3}q_3 \quad u_3 = R_{32b}q_{2b} + R_{33}q_3 \end{aligned} \tag{7}$$

For this stepped shaft example, a rigid connection is applied at the interface. The corresponding compatibility conditions are:

$$u_2 - u_{2b} = 0 \text{and} u_i = U_i \tag{8}$$

where i = 1–3 and the latter expression specifies that the component and assembly coordinates are defined at the same spatial positions. The equilibrium conditions vary with the external force/moment location. To determine the first column of the assembly receptance matrix in Eq. (6), Q_1 is applied to coordinate U_1. In this case, the equilibrium conditions are:

$$q_2 + q_{2b} = 0, q_1 = Q_1, \text{and} q_3 = 0 \tag{9}$$

Substitution of the component displacements/rotations and equilibrium conditions into the compatibility conditions yields q_2; see Eq. (10). The expression for G_{11} is then given by Eq. (11). The other two first column receptances are determined in a similar manner. To find the receptances in the second and third columns, Q_2 must be applied to U_2 and Q_3 to U_3, respectively.

$$q_2 = -(R_{22} + R_{2b2b})^{-1}R_{21}Q_1 \tag{10}$$

$$\begin{aligned} G_{11} &= \frac{U_1}{Q_1} = \frac{u_1}{Q_1} = \frac{R_{11}q_1 + R_{12}q_2}{Q_1} \\ G_{11} &= R_{11} - R_{12}(R_{22} + R_{2b2b})^{-1}R_{21} = \begin{bmatrix} H_{11} & L_{11} \\ N_{11} & P_{11} \end{bmatrix} \end{aligned} \tag{11}$$

Multi-point RCSA

This paper extends the single point (end-to-end) RCSA procedure to enable multiple coupling locations between the external surface of the tool inside the holder and the internal surface of the holder that clamps the tool. To demonstrate the coupling method, consider a rigid connection between a free-free internal cylinder and free-free external tube, where the internal cylinder's outer diameter is equal to the inner diameter of the external tube. Here, it is not sufficient to couple the two components only at their endpoints. The relative motions at coordinates along the assembly axis must also be constrained. The case of three connection coordinates (3-point coupling), located at the assembly ends and at mid-length, is described here. This gives a total of six component coordinates – three each on the internal cylinder and external tube; see Fig. 3.

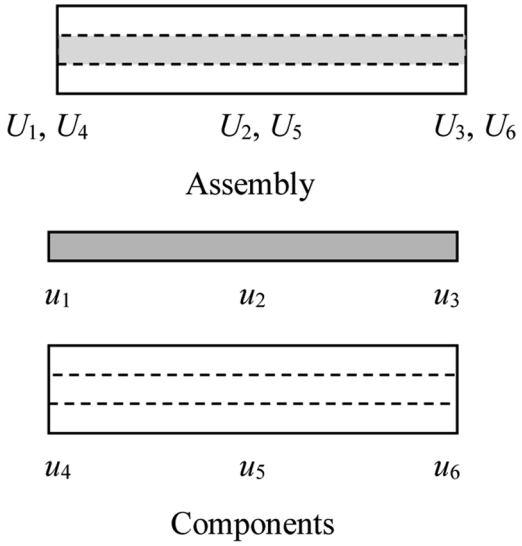

Fig. 3. Cylinder-in-tube assembly (top) and components (bottom).

The component displacement/rotations are written as shown in Eq. (12).

$$\begin{aligned} u_1 &= R_{11}q_1 + R_{12}q_2 + R_{13}q_3 \quad u_2 = R_{21}q_1 + R_{22}q_2 + R_{23}q_3 \\ u_3 &= R_{31}q_1 + R_{32}q_2 + R_{33}q_3 \quad u_4 = R_{44}q_4 + R_{45}q_5 + R_{46}q_6 \\ u_5 &= R_{54}q_4 + R_{55}q_5 + R_{56}q_6 \quad u_6 = R_{64}q_4 + R_{65}q_5 + R_{66}q_6 \end{aligned} \tag{12}$$

The compatibility conditions for the rigid connections are:

$$u_1 - u_4 = 0, u_2 - u_5 = 0, \text{and} u_3 - u_6 = 0 \tag{13}$$

and the component and assembly coordinates are defined at the same spatial locations so that $u_i = U_i$, $i = 1$–6. If the assembly direct response, $G_{11}(\omega)$, at the left end on the cylinder is to be determined, Q_1 is applied to coordinate U_1 of the assembly. The equilibrium conditions are then:

$$q_1 + q_4 = Q_1, q_2 + q_5 = 0, \text{and} q_3 + q_6 = 0 \tag{14}$$

G_{11} is determined using a matrix representation of the relevant equations. The first step is to insert the component displacement/rotation expressions into the compatibility conditions; Eq. (15).

$$\begin{aligned} R_{11}q_1 + R_{12}q_2 + R_{13}q_3 &= R_{44}q_4 + R_{45}q_5 + R_{46}q_6 \\ R_{21}q_1 + R_{22}q_2 + R_{23}q_3 &= R_{54}q_4 + R_{55}q_5 + R_{56}q_6 \\ R_{31}q_1 + R_{32}q_2 + R_{33}q_3 &= R_{64}q_4 + R_{65}q_5 + R_{66}q_6 \end{aligned} \tag{15}$$

The next step is to substitute $q_4 = Q_1 - q_1$, $q_5 = -q_2$, and $q_6 = -q_3$ and rearrange to obtain Eq. (16).

$$\begin{bmatrix} R_{11}+R_{44} & R_{12}+R_{45} & R_{13}+R_{46} \\ R_{21}+R_{54} & R_{22}+R_{55} & R_{23}+R_{56} \\ R_{31}+R_{64} & R_{32}+R_{65} & R_{33}+R_{66} \end{bmatrix} \begin{Bmatrix} q_1 \\ q_2 \\ q_3 \end{Bmatrix} = \begin{bmatrix} R_{44} \\ R_{54} \\ R_{64} \end{bmatrix} \begin{Bmatrix} Q_1 \\ Q_2 \\ Q_3 \end{Bmatrix} \tag{16}$$

This gives the relationship between the component forces/moments and externally applied force/moment in matrix form. For this example, G_{11} can be expressed as:

$$G_{11} = \frac{U_1}{Q_1} = \frac{u_1}{Q_1} = R_{11}\frac{q_1}{Q_1} + R_{12}\frac{q_2}{Q_1} + R_{13}\frac{q_3}{Q_1} \tag{17}$$

so the ratios $\frac{q_1}{Q_1}$, $\frac{q_2}{Q_1}$, and $\frac{q_3}{Q_1}$ are required. These can be determined by rearranging Eq. (16) as shown in Eq. (18).

$$\begin{Bmatrix} q_1 \\ q_2 \\ q_3 \end{Bmatrix} \begin{Bmatrix} Q_1 \\ Q_2 \\ Q_3 \end{Bmatrix}^{-1} = \begin{bmatrix} R_{11}+R_{44} & R_{12}+R_{45} & R_{13}+R_{46} \\ R_{21}+R_{54} & R_{22}+R_{55} & R_{23}+R_{56} \\ R_{31}+R_{64} & R_{32}+R_{65} & R_{33}+R_{66} \end{bmatrix}^{-1} \begin{bmatrix} R_{44} \\ R_{54} \\ R_{64} \end{bmatrix}$$
$$\begin{Bmatrix} q_1 \\ q_2 \\ q_3 \end{Bmatrix} \begin{Bmatrix} Q_1 \\ Q_2 \\ Q_3 \end{Bmatrix}^{-1} = [A] \tag{18}$$

In this equation, $[A]$ is a 6×2, or $2n \times 2$, by N matrix (N is the number of points in the frequency vector, ω). The reader may note that the matrix size is 6×2 because R_{ij} is a 2×2 matrix. The matrix A is partitioned as follows: the first two rows of A give $\frac{q_1}{Q_1}$; the second two rows provide $\frac{q_2}{Q_1}$; and the final two rows give $\frac{q_3}{Q_1}$. The desired direct receptances can then be computed from Eq. (17).

This 3-point coupling example can be extended to n coupling points by recognizing the recursive pattern in Eq. (18). Note that a larger number of coupling points enables higher order modes to be modeled. The number of accurately modeled mode shapes is equal to n-2 for free-free beams. This is demonstrated in Fig. 5. If the coupling coordinates are equally spaced, only the first mode shape can be accurately modeled for three coupling coordinates. The second mode shape has the middle coordinate located at a node and the third does not have an adequate number of points to identify the shape.

If the Fig. 4 coordinate numbering scheme is observed for n-point coupling points, the A matrix for this general case is given by Eq. (19).

$$[A] = \begin{bmatrix} R_{11}+R_{n+1,n+1} & R_{12}+R_{n+1,n+2} & \cdots & R_{1n}+R_{n+1,2n} \\ R_{21}+R_{n+2,n+1} & R_{22}+R_{n+2,n+2} & \cdots & R_{2n}+R_{n+2,2n} \\ \vdots & \vdots & \ddots & \vdots \\ R_{n1}+R_{2n,n+1} & R_{n2}+R_{2n,n+2} & \cdots & R_{nn}+R_{2n,2n} \end{bmatrix}^{-1} \begin{bmatrix} R_{n+1,n+1} \\ R_{n+2,n+1} \\ \vdots \\ R_{2n,n+1} \end{bmatrix} \tag{19}$$

The $[A]$ matrix can again be partitioned to find $\frac{q_1}{Q_1}$, $\frac{q_2}{Q_1}$, … $\frac{q_n}{Q_1}$. The assembly receptances G_{11} can then be found using Eq. (20). The required receptances, R_{ij}, for the inner cylinder and outer tube are calculated using the closed form Euler-Bernoulli free-free beam receptances described by Bishop and Johnson, where the beam lengths are defined by the coordinate locations [118]. Additional details for defining the A matrix receptances are provided in [20].

$$G_{11} = R_{11}\frac{q_1}{Q_1} + R_{12}\frac{q_2}{Q_1} + \ldots + R_{1n}\frac{q_n}{Q_1} \tag{20}$$

In the case of finite stiffness and non-zero damping at the contact interface between the inner tool and outer holder, the compatibility conditions can be modified to reflect the new coordinate displacement/rotation relationships. To demonstrate, the 3-point inner cylinder-outer tube (free-free boundary condition) coupling shown in Fig. 3 is modified.

The compatibility conditions for the flexible-damped connection are now:

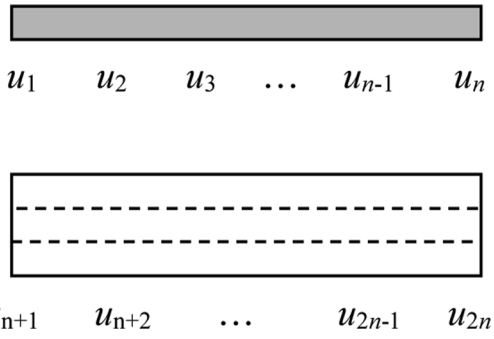

Fig. 4. Cylinder-in-tube component coordinates for n-point coupling.

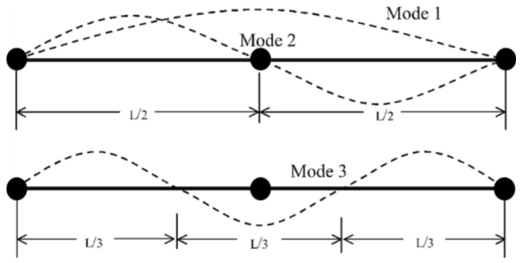

Fig. 5. First three modes shapes for free-free boundary condition beam.

$$K(u_4 - u_1) = -q_4, K(u_5 - u_2) = -q_5, \text{ and} K(u_6 - u_3) = -q_6 \quad (21)$$

where the complex stiffness matrix is defined in Eq. (22) for a viscous damping model. In this matrix, the stiffness and damping terms are defined by their subscripts. The k_{xf} term, for example, describes the stiffness that relates force to displacement, while the stiffness $k_{\theta m}$ relates rotation to moment.

$$K = \begin{bmatrix} k_{xf} + i\omega c_{xf} & k_{\theta f} + i\omega c_{\theta f} \\ k_{xm} + i\omega c_{xm} & k_{\theta m} + i\omega c_{\theta m} \end{bmatrix} \quad (22)$$

To find the direct receptances at the left end of the 3-point coupled assembly, Q_1 is again applied to U_1 (the corresponding equilibrium conditions are provided in Eq. (14)). After inserting the component displacement/rotation expressions (Eq. (12)) and equilibrium conditions into Eq. (21) and rearranging, a modified version of Eq. (18) is obtained, where the complex stiffness matrix now appears. The solution procedure for the assembly receptances and derivation of the component receptances remain the same.

$$\begin{Bmatrix} q_1 \\ q_2 \\ q_3 \end{Bmatrix} \begin{Bmatrix} Q_1 \\ Q_2 \\ Q_3 \end{Bmatrix}^{-1} = \begin{bmatrix} R_{11} + R_{44} + K^{-1} & R_{12} + R_{45} & R_{13} + R_{46} \\ R_{21} + R_{54} & R_{22} + R_{55} + K^{-1} & R_{23} + R_{56} \\ R_{31} + R_{64} & R_{32} + R_{65} & R_{33} + R_{66} + K^{-1} \end{bmatrix}^{-1} \times \begin{bmatrix} R_{44} + K^{-1} \\ R_{54} \\ R_{64} \end{bmatrix} = [A] \quad (23)$$

Experimental setup

Measurements were completed using the spindle test stand. This is a large steel block with a manual draw bolt that enables the tapered holder to be clamped in the corresponding spindle taper. For this testing, a CAT-40 holder-spindle interface was used. The full RCSA procedure included six steps:

1 The spindle-artifact receptances were measured using a standard geometry artifact. The four direct receptances at the free end of the artifact were determined from a single displacement-to-force measurement as described in [58]. All measurements were performed by impact testing, where an instrumented modal hammer was used to excite the structure over the desired bandwidth and the response was measured using a low mass accelerometer. A photograph of the cylindrical artifact clamped in the spindle test stand is provided in Fig. 6.

2 The spindle receptances were then determined from the spindle-artifact receptances using the inverse RCSA approach detailed in [14]. In this method, the assembly receptances are measured and then the free-free portion of the artifact beyond the holder flange is extracted to isolate the spindle receptances; see Fig. 7.

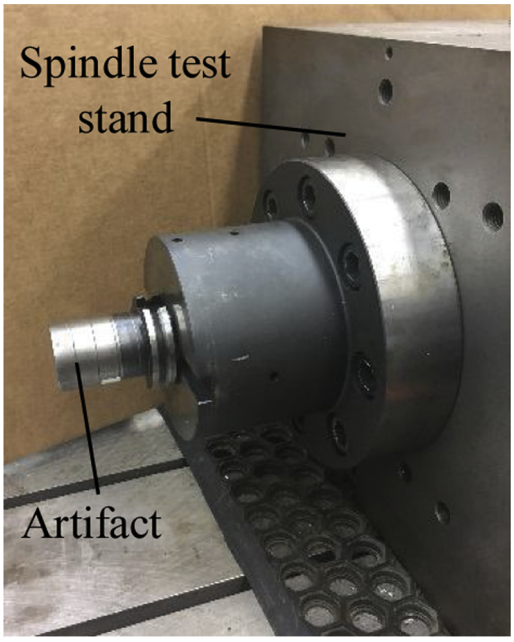

Fig. 6. Photograph of artifact clamped in the spindle test stand.

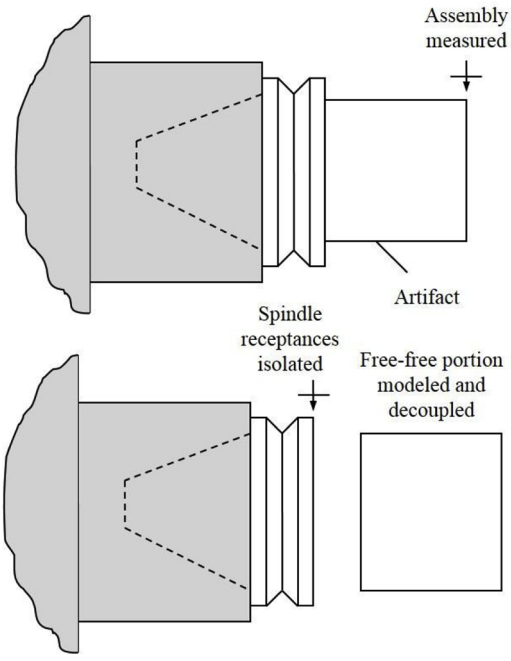

Fig. 7. Spindle receptances were determined using inverse RCSA.

3 Once the spindle receptances were known at the holder-flange, they were rigidly coupled to the portion of the holder with no tool inside (free-free boundary conditions). The holder used for this study was a Parlec C40-32ERP412 collet holder (ER32 tool-holder connection). The portion of the holder with no tool inside had an outer diameter of 44.3 mm, inner diameter of 19 mm, and length of 43 mm. The material was steel with an assumed elastic modulus of 200 GPa, density of 7800 kg/m^3, and solid damping factor of 0.0015. These parameters were applied to identify the free-free receptances using the Euler-Bernoulli beam receptances described by Eq. (4).

4 The portion of the holder with the tool inside and the portion of the tool clamped inside the holder were then modeled using the free-free boundary condition Euler-Bernoulli beam receptances and coupled at seven equally spaced locations (i.e., 7-point coupling).

Table 1
Tool blank diameters and extension lengths.

Diameter (mm)	Length (mm)	Diameter (mm)	Length (mm)
6.35	24.21	12.7	37.03
6.35	37.25	12.7	62.57
6.35	49.66	12.7	87.26
–	–	12.7	112.70
–	–	12.7	138.30
–	–	12.7	163.12
15.875	63.49	19.05	74.85
15.875	94.60	19.05	113.77
15.875	127.23	19.05	151.93
15.875	170.06	–	–

The length of this section was 40 mm (collet length) and the outer diameter was 47.47 mm. The outer holder portion was steel, while the inner tool portion was carbide. The assumed carbide elastic modulus was 550 GPa, the density was 14400 kg/m^3, and solid damping factor was 0.0015. The inner diameter for this section was the carbide tool blank diameter. The complex stiffness matrix defined in Eq. (22) was applied at each of the seven coupling locations.

5 The free-free 7-point coupling result from 4 was then rigidly coupled to the result from 3.

6 Finally, the result from 5 was rigidly coupled to the portion of the carbide tool blank that extended outside the holder. The final result was the tool point receptance, which was visually compared to the measured results to identify the best-fit complex stiffness matrix. The length and diameter of the tool blank were varied as part of this study; see Table 1. In all cases, however, the tool blank was fully inserted in the collet so the insertion length was always 40 mm. A photograph of an example tool assembly is provided in Fig. 8. RCSA coordinates are identified in Fig. 9.

Experimental results

Impact tests were performed for the 16 tool blank diameter-extension length combinations provided in Table 1. For each diameter, a single complex stiffness matrix was defined (four stiffness and four viscous damping values) to predict the tool point receptance for each tool blank extension length. The results are provided individually for each diameter in the following sections.

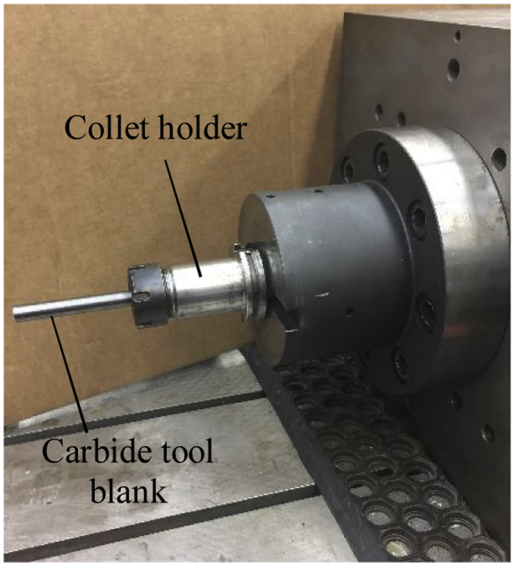

Fig. 8. Photograph of tool-holder clamped in the spindle test stand.

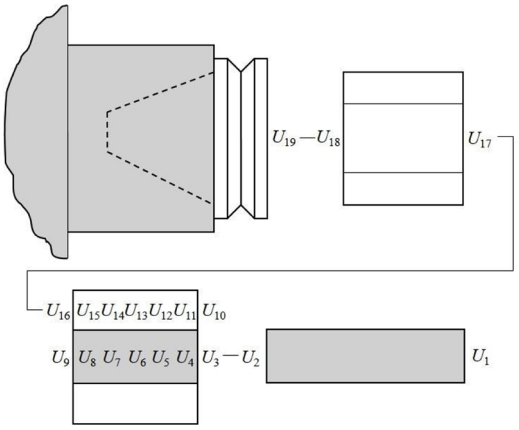

Fig. 9. RCSA coupling coordinates from the spindle (U_{19}) to the tool point (U_1). The direct tool point receptance was predicted using 7-point coupling for comparison to measurement.

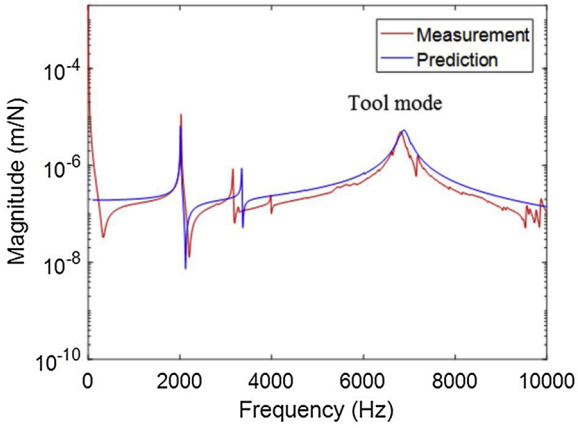

Fig. 10. 6.35 mm diameter tool with 24.21 mm length.

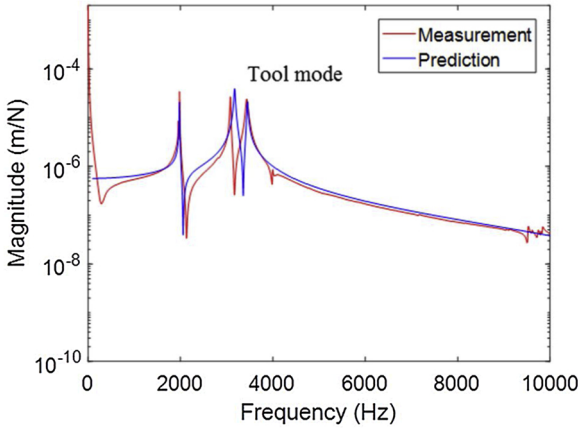

Fig. 11. 6.35 mm diameter tool with 37.25 mm length.

6.35. mm diameter

The tool point displacement-to-force receptance predictions and measurements for the 6.35 mm carbide tool blanks are displayed in Figs. 10–12. A semilog scale is applied to enable the multiple modes with large differences in magnitudes to be observed. The tool's cantilever bending mode is identified in each case. The stiffness matrix used to predict the tool point receptances is shown in Eq. (24).

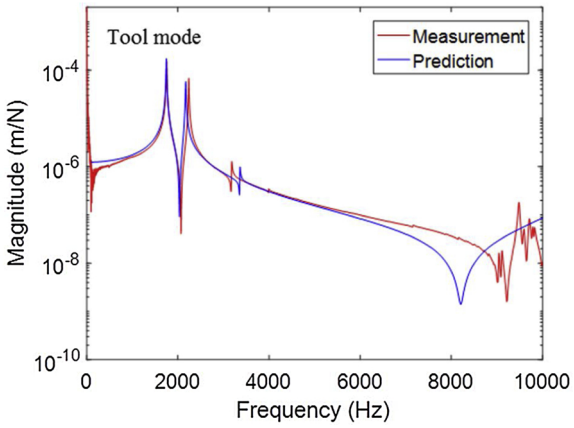

Fig. 12. 6.35 mm diameter tool with 49.66 mm length.

$$K = \begin{bmatrix} 1 \times 10^7 + i\omega 0.1 & 1 \times 10^6 \\ 1 \times 10^6 & 3.9 \times 10^3 + i\omega 0.01 \end{bmatrix} \quad (24)$$

12.7. mm diameter

The tool point displacement-to-force receptance predictions and measurements for the 12.7 mm carbide tool blanks are displayed in Figs. 13–18. The stiffness matrix used to predict the tool point receptance is shown in Eq. (25).

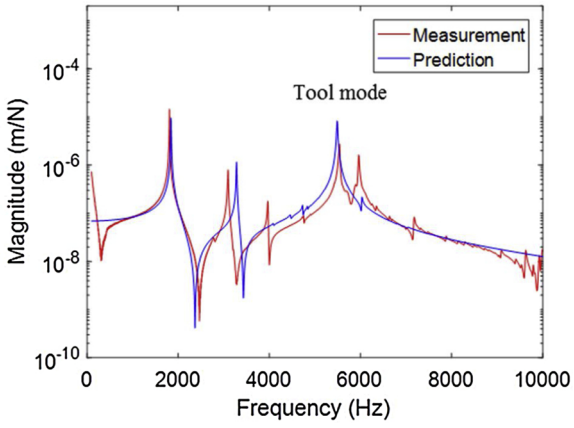

Fig. 13. 12.7 mm diameter tool with 37.03 mm length.

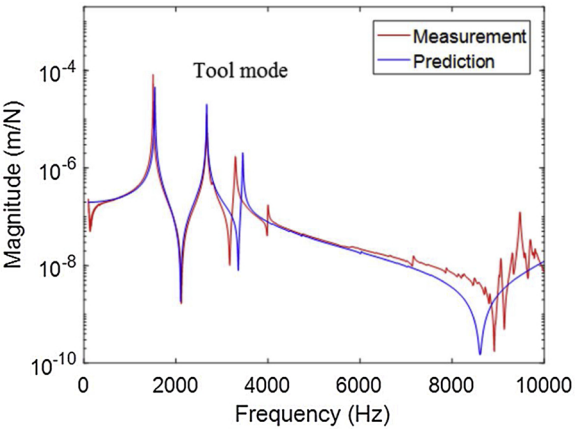

Fig. 14. 12.7 mm diameter tool with 62.57 mm length.

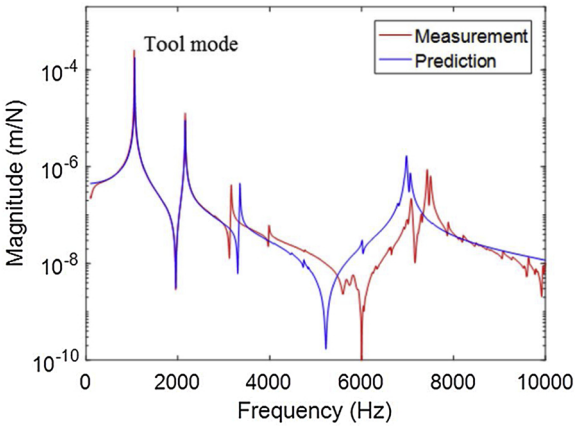

Fig. 15. 12.7 mm diameter tool with 87.26 mm length.

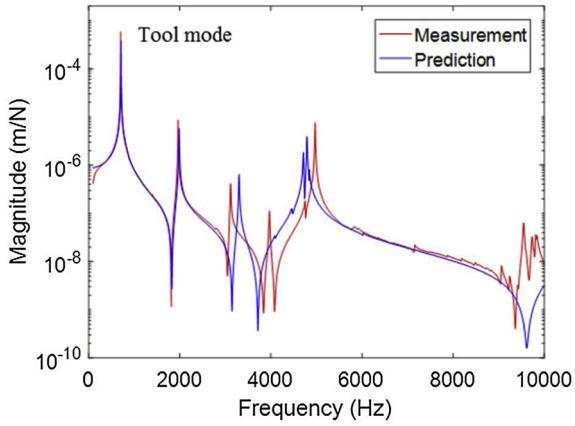

Fig. 16. 12.7 mm diameter tool with 112.70 mm length.

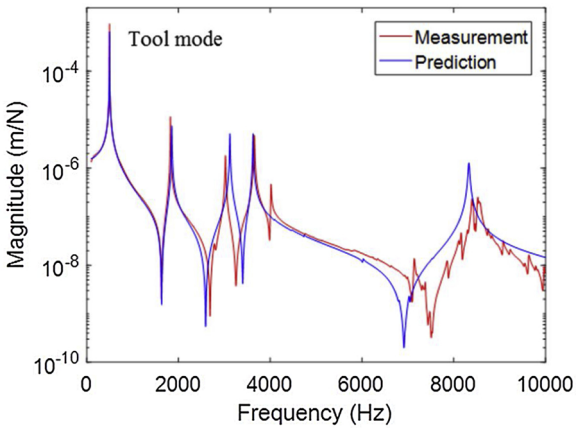

Fig. 17. 12.7 mm diameter tool with 138.30 mm length.

$$K = \begin{bmatrix} 1 \times 10^7 + i\omega 0.1 & 1 \times 10^6 \\ 1 \times 10^6 & 3.5 \times 10^4 + i\omega 0.01 \end{bmatrix} \quad (25)$$

15.875. mm diameter

The tool point displacement-to-force receptance predictions and measurements for the 15.875 mm carbide tool blanks are displayed in Figs. 19–22. The stiffness matrix used to predict the tool point receptance is shown in Eq. (26).

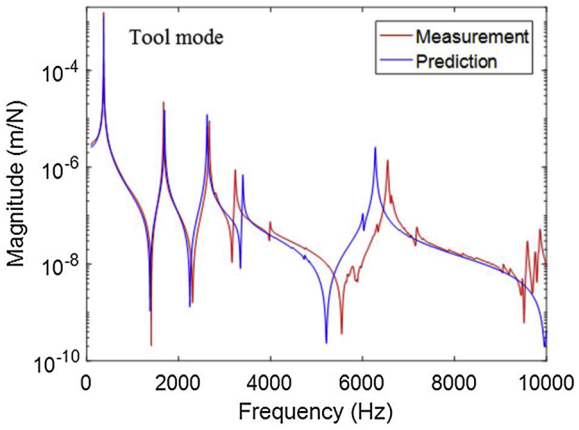

Fig. 18. 12.7 mm diameter tool with 163.12 mm length.

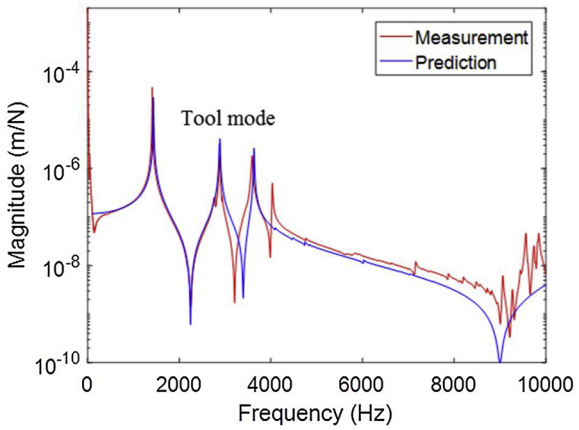

Fig. 19. 15.875 mm diameter tool with 63.49 mm length.

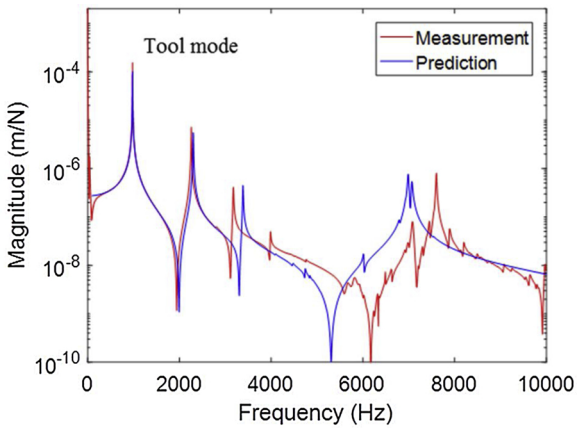

Fig. 20. 15.875 mm diameter tool with 94.60 mm length.

$$K = \begin{bmatrix} 1 \times 10^7 + i\omega 0.1 & 1 \times 10^6 \\ 1 \times 10^6 & 4.5 \times 10^4 + i\omega 0.01 \end{bmatrix} \quad (26)$$

19.05. mm diameter

The tool point displacement-to-force receptance predictions and measurements for the 19.05 mm carbide tool blanks are displayed in Figs. 23–25. The stiffness matrix used to predict the tool point receptance is shown in Eq. (27).

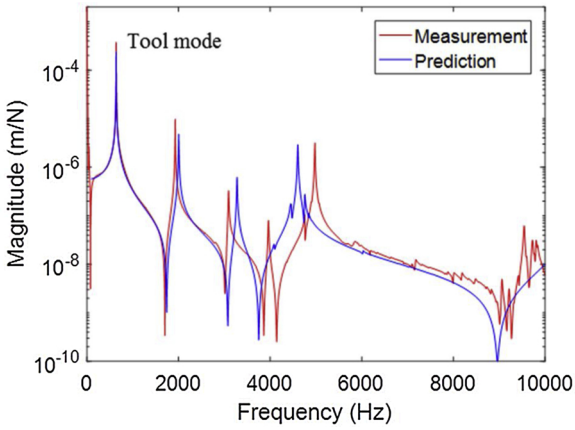

Fig. 21. 15.875 mm diameter tool with 127.23 mm length.

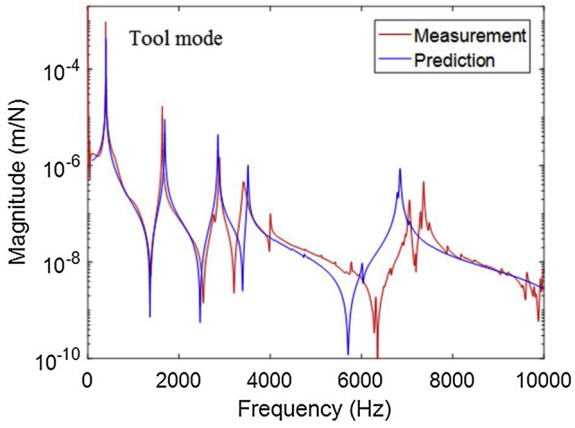

Fig. 22. 15.875 mm diameter tool with 170.06 mm length.

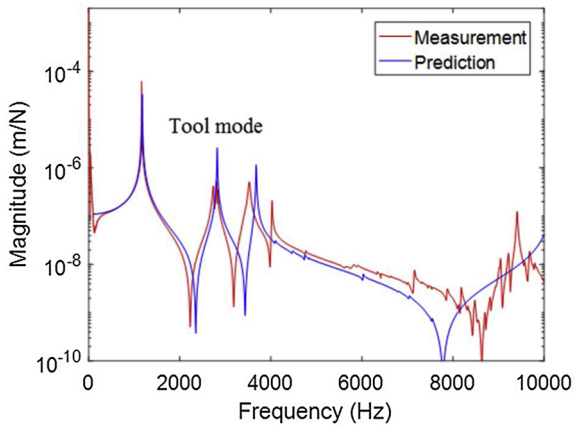

Fig. 23. 19.05 mm diameter tool with 74.85 mm length.

$$K = \begin{bmatrix} 1 \times 10^7 + i\omega 0.1 & 1 \times 10^6 \\ 1 \times 10^6 & 5 \times 10^4 + i\omega 0.01 \end{bmatrix} \quad (27)$$

In all 16 cases, the 7-point coupling model was able to predict the tool point receptance with acceptable accuracy. The stiffness matrices provided in Eqs. (24)–(27) differed in only one of the eight terms, $k_{\theta m}$, the stiffness entry that relates rotation to moment. The variation in this value with diameter is displayed in Fig. 26. The data points are the circles and the quadratic fit is the dashed curve. The fit is described by Eq. 28 and the corresponding coefficient of determination (R^2 value) is 0.9999.

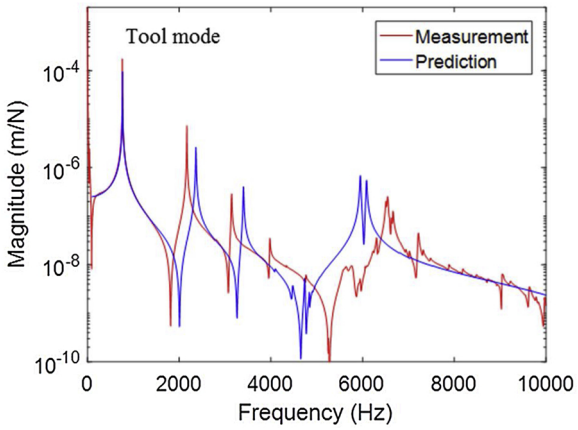

Fig. 24. 19.05 mm diameter tool with 113.77 mm length.

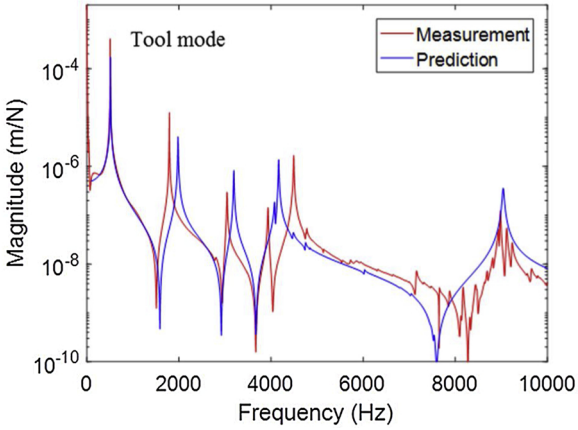

Fig. 25. 19.05 mm diameter tool with 151.93 mm length.

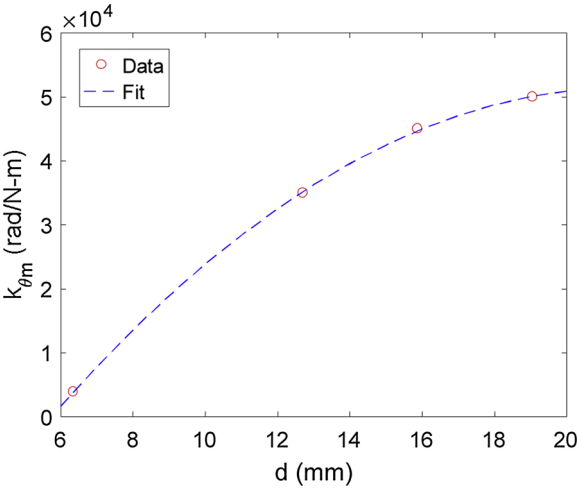

Fig. 26. Second-order variation in the rotation-to-moment stiffness with tool blank diameter.

$$k_{\theta m} = ad^2 + bd + c \text{ (rad/ N– m)} \quad (28)$$

In this equation, d is the tool blank diameter in mm, a = -284 (-336.2, -71.85), b = 8824 (5488, 12160), and c = -43940 (-62870, -25010). For the fitting parameters a-c, the mean value is listed immediately after the equal sign and the 95% confidence bounds are provided parenthetically.

Conclusions

This paper described a multi-point receptance coupling substructure analysis (RCSA) technique for predicting the tool point frequency response function using a measurement of the spindle and models of the holder and tool. In this approach, the portion of the tool inside the holder was coupled to the portion of the holder that clamps the tool at multiple equally spaced points along the insertion length. A flexible-damped coupling matrix was employed and was populated using the analytical RCSA model together with experiments. Four carbide tool blank diameters were tested at 16 total extension lengths using an ER32 collet connection. It was determined that a second-order dependence of the rotation-to-moment stiffness term on tool blank diameter was sufficient to accurately predict all diameter-length combinations. All other terms in the complex stiffness matrix were kept constant. The value of predicting the tool point receptance is that milling process models can then be used to selected optimized operating parameters at the process planning stage.

Acknowledgements

This material is based on work supported by the National Science Foundation under Grant No. CMMI-1561221.

References

[1] Schmitz TL, Smith KS. Machining dynamics: frequency response to improved productivity. New York, NY: Springer; 2009.
[2] Schmitz TL, Donaldson RR. Predicting high-speed machining dynamics by substructure analysis. CIRP Annals-Manufacturing Technology 2000;49(1):303–8.
[3] Schmitz T, Davies M, Kennedy M. High-speed machining frequency response prediction for process optimization. Proceedings of the 2nd International Seminar on Improving Machine Tool Performance 2000:3–5.
[4] Schmitz TL, Davies MA, Kennedy MD. Tool point frequency response prediction for high-speed machining by RCSA. J Manuf Sci Eng 2001;123(4):700–7.
[5] Schmitz TL, Davies MA, Medicus K, Snyder J. Improving high-speed machining material removal rates by rapid dynamic analysis. CIRP Annals-Manufacturing Technology 2001;50(1):263–8.
[6] Choi BL, Park JM. An improved rotor model with equivalent dynamic effects of the support structure. J Sound Vib 2001;244(4):569–81.
[7] Schmitz T, Burns T. Receptance coupling for high-speed machining dynamics prediction. Proceedings of the 21st International Modal Analysis Conference 2003;vol. 36.
[8] Park SS, Altintas Y, Movahhedy M. Receptance coupling for end mills. Int J Mach Tools Manuf 2003;43(9):889–96.
[9] Yang T, Fan SH, Lin CS. Joint stiffness identification using FRF measurements. Comput Struct 2003;81(28–29):2549–56.
[10] Schmitz TL, Burns TJ, Ziegert JC, Dutterer B, Winfough WR. Tool length-dependent stability surfaces. Mach Sci Technol 2004;8(3):377–97.
[11] Burns TJ, Schmitz TL. Receptance coupling study of tool-length dependent dynamic absorber effect. ASME 2004 International Mechanical Engineering Congress and Exposition 2004:993–1000.
[12] Schmitz TL. Improved sensor data utility through receptance coupling modeling. ASME 2004 International Mechanical Engineering Congress and Exposition 2004:411–7.
[13] Kivanc EB, Budak E. Structural modeling of end mills for form error and stability analysis. Int J Mach Tools Manuf 2004;44(11):1151–61.
[14] Schmitz TL, Duncan GS. Three-component receptance coupling substructure analysis for tool point dynamics prediction. J Manuf Sci Eng 2005;127(4):781–90.
[15] Burns TJ, Schmitz TL. A study of linear joint and tool models in spindle-holder-tool receptance coupling. ASME 2005 International Design Engineering Technical Conferences and Computers and Information in Engineering Conference 2005:947–54.
[16] Duncan GS, Tummond MF, Schmitz TL. An investigation of the dynamic absorber effect in high-speed machining. Int J Mach Tools Manuf 2005;45(4-5):497–507.
[17] Duncan GS, Schmitz T. An improved RCSA model for tool point frequency response prediction. Proceedings of the 23rd International Modal Analysis Conference 2005;vol. 30.
[18] Cheng CH, Schmitz TL, Arakere N, Duncan GS. An approach for micro end mill frequency response predictions. ASME 2005 International Mechanical Engineering Congress and Exposition 2005:1139–45.
[19] Tekeli A, Budak E. Maximization of chatter-free material removal rate in end milling using analytical methods. Mach Sci Technol 2005;9(2):147–67.
[20] Schmitz TL, Duncan GS. Receptance coupling for dynamics prediction of assemblies with coincident neutral axes. J Sound Vib 2006;289(4-5):1045–65.
[21] Budak E. Analytical models for high performance milling. Part II: process dynamics and stability. Int J Mach Tools Manuf 2006;46(12–13):1489–99.
[22] Lee SW, Mayor R, Ni J. Dynamic analysis of a mesoscale machine tool. J Manuf Sci

Eng 2006;128(1):194–203.
[23] Ertürk A, Özgüven HN, Budak E. Analytical modeling of spindle-tool dynamics on machine tools using Timoshenko beam model and receptance coupling for the prediction of tool point FRF. Int J Mach Tools Manuf 2006;46(15):1901–12.
[24] Ertürk A, Özgüven H, Budak E. Analytical modeling of spindle–tool dynamics on machine tools using Timoshenko beam model and receptance coupling for the prediction of tool point FRF. Int J Mach Tools Manuf 2006;46(15).
[25] Budak E, Ertürk A, Özgüven HN. A modeling approach for analysis and improvement of spindle-holder-tool assembly dynamics. CIRP Annals-Manufacturing Technology 2006;55(1):369–72.
[26] Park SS. Identification of spindle integrated force sensor's transfer function for modular end mills. J Manuf Sci Eng 2006;128(1):146–53.
[27] Movahhedy MR, Gerami JM. Prediction of spindle dynamics in milling by substructure coupling. Int J Mach Tools Manuf 2006;46(3-4):243–51.
[28] Koplow MA, Bhattacharyya A, Mann BP. Closed form solutions for the dynamic response of Euler-Bernoulli beams with step changes in cross section. J Sound Vib 2006;295(1-2):214–25.
[29] Mascardelli BA, Park SS, Freiheit T. Substructure coupling of micro-end mills. ASME 2006 International Mechanical Engineering Congress and Exposition 2006:145–50.
[30] Schmitz TL, Powell K, Won D, Duncan GS, Sawyer WG, Ziegert JC. Shrink fit tool holder connection stiffness/damping modeling for frequency response prediction in milling. Int J Mach Tools Manuf 2007;47(9):1368–80.
[31] Cheng CH, Schmitz TL, Scott Duncan G. Rotating tool point frequency response prediction using RCSA. Mach Sci Technol 2007;11(3):433–46.
[32] Ertürk A, Budak E, Özgüven HN. Selection of design and operational parameters in spindle–holder–tool assemblies for maximum chatter stability by using a new analytical model. Int J Mach Tools Manuf 2007;47(9):1401–9.
[33] Namazi M, Altintas Y, Abe T, Rajapakse N. Modeling and identification of tool holder–spindle interface dynamics. Int J Mach Tools Manuf 2007;47(9):1333–41.
[34] Ahmadi K, Ahmadian H. Modelling machine tool dynamics using a distributed parameter tool–holder joint interface. Int J Mach Tools Manuf 2007;47(12–13):1916–28.
[35] Ertürk A, Özgüven HN, Budak E. Effect analysis of bearing and interface dynamics on tool point FRF for chatter stability in machine tools by using a new analytical model for spindle–tool assemblies. Int J Mach Tools Manuf 2007;47(1):23–32.
[36] Houming Z, Chengyong W, Zhenyu Z. Dynamic characteristics of conjunction of lengthened shrink-fit holder and cutting tool in high-speed milling. J Mater Process Technol 2008;207(1-3):154–62.
[37] Park SS, Chae J. Joint identification of modular tools using a novel receptance coupling method. Int J Adv Manuf Technol 2008;35(11–12):1251–62.
[38] Mascardelli BA, Park SS, Freiheit T. Substructure coupling of microend mills to aid in the suppression of chatter. J Manuf Sci Eng 2008;130(1):011010.
[39] Lin SY, Fang YC, Huang CW. Improvement strategy for machine tool vibration induced from the movement of a counterweight during machining process. Int J Mach Tools Manuf 2008;48(7-8):870–7.
[40] Özşahin O, Budak E, Özgüven HN. Estimation of dynamic contact parameters for machine tool spindle-holder-tool assemblies using artificial neural networks. Proceedings of the 3rd International Conference on Manufacturing Engineering (ICMEN). 2008. p. 131–44.
[41] Filiz S, Cheng CH, Powell KB, Schmitz TL, Ozdoganlar OB. An improved tool-holder model for RCSA tool-point frequency response prediction. Precis Eng 2009;33(1):26–36.
[42] Park SS, Malekian M. Mechanistic modeling and accurate measurement of micro end milling forces. CIRP Ann Manuf Technol 2009;58(1):49–52.
[43] Rahnama R, Sajjadi M, Park SS. Chatter suppression in micro end milling with process damping. J Mater Process Technol 2009;209(17):5766–76.
[44] Özşahin O, Ertürk A, Özgüven HN, Budak E. A closed-form approach for identification of dynamical contact parameters in spindle-holder-tool assemblies. Int J Mach Tools Manuf 2009;49(1):25–35.
[45] Banerjee A, Bordatchev EV, Feng HY. Determination of minimum limiting axial depth of cut for 2½D pocket machining based on receptance coupling. Mach Sci Technol 2009;13(2):177–95.
[46] Malekian M, Park SS, Jun MB. Modeling of dynamic micro-milling cutting forces. Int J Mach Tools Manuf 2009;49(7-8):586–98.
[47] Schmitz TL. Torsional and axial frequency response prediction by RCSA. Precis Eng 2010;34(2):345–56.
[48] Novakov T, Jackson MJ. Chatter problems in micro-and macrocutting operations, existing models, and influential parameters – a review. Int J Adv Manuf Technol 2010;47(5-8):597–620.
[49] Wang H, To S, Chan CY, Cheung CF, Lee WB. A theoretical and experimental investigation of the tool-tip vibration and its influence upon surface generation in single-point diamond turning. Int J Mach Tools Manuf 2010;50(3):241–52.
[50] Park SS, Rahnama R. Robust chatter stability in micro-milling operations. CIRP Ann Manuf Technol 2010;59(1):391–4.
[51] Zhang J, Schmitz T, Zhao W, Lu B. Receptance coupling for tool point dynamics prediction on machine tools. Chinese Journal of Mechanical Engineering-English Edition 2011;24(3):340.
[52] Ding Y, Zhu L, Zhang X, Ding H. On a numerical method for simultaneous prediction of stability and surface location error in low radial immersion milling. J Dyn Syst Meas Control 2011;133(2):024503.
[53] Mancisidor I, Zatarain M, Munoa J, Dombovari Z. Fixed boundaries receptance coupling substructure analysis for tool point dynamics prediction. Advanced materials research vol. 223. Trans Tech Publications; 2011. p. 622–31.
[54] Mancisidor I, Zatarain M, Munoa J, Dombovari Z. Receptance coupling for tool point dynamics prediction. In 17th CIRP International Conference on Modelling of Machining Operations. 2011, May.
[55] Kolar P, Sulitka M, Janota M. Simulation of dynamic properties of a spindle and tool system coupled with a machine tool frame. Int J Adv Manuf Technol 2011;54(1-4):11–20.
[56] Forestier F, Gagnol V, Ray P, Paris H. Model-based operating recommendations for high-speed spindles equipped with a self-vibratory drilling head. Mech Mach Theory 2011;46(11):1610–22.
[57] Mehrpouya M, Park SS. Prediction of atomic force microscope probe dynamics through the receptance coupling method. Rev Sci Instrum 2011;82(12):125001.
[58] Kumar UV, Schmitz TL. Spindle dynamics identification for receptance coupling substructure analysis. Precis Eng 2012;36(3):435–43.
[59] Bediz B, Kumar U, Schmitz TL, Ozdoganlar OB. Modeling and experimentation for three-dimensional dynamics of endmills. Int J Mach Tools Manuf 2012;53(1):39–50.
[60] Ozturk E, Kumar U, Turner S, Schmitz T. Investigation of spindle bearing preload on dynamics and stability limit in milling. CIRP Annals-Manufacturing Technology 2012;61(1):343–6.
[61] Rezaei MM, Movahhedy MR, Moradi H, Ahmadian MT. Extending the inverse receptance coupling method for prediction of tool-holder joint dynamics in milling. J Manuf Process 2012;14(3):199–207.
[62] Afazov SM, Ratchev SM, Segal J, Popov AA. Chatter modelling in micro-milling by considering process nonlinearities. Int J Mach Tools Manuf 2012;56:28–38.
[63] Albertelli P, Cau N, Bianchi G, Monno M. The effects of dynamic interaction between machine tool subsystems on cutting process stability. Int J Adv Manuf Technol 2012;58(9–12):923–32.
[64] Forestier F, Gagnol V, Ray P, Paris H. Model-based cutting prediction for a self-vibratory drilling head-spindle system. Int J Mach Tools Manuf 2012;52(1):59–68.
[65] Budak E, Tunç LT, Alan S, Özgüven HN. Prediction of workpiece dynamics and its effects on chatter stability in milling. CIRP Annals-Manufacturing Technology 2012;61(1):339–42.
[66] Cao H, Li B, He Z. Chatter stability of milling with speed-varying dynamics of spindles. Int J Mach Tools Manuf 2012;52(1):50–8.
[67] Altintas Y. Manufacturing automation: metal cutting mechanics, machine tool vibrations, and CNC design. Cambridge university press; 2012.
[68] Ganguly V, Schmitz TL. Spindle dynamics identification using particle swarm optimization. J Manuf Process 2013;15(4):444–51.
[69] Cao H, Li B, He Z. Finite element model updating of machine-tool spindle systems. J Vib Acoust 2013;135(2):024503.
[70] Albertelli P, Goletti M, Monno M. A new receptance coupling substructure analysis methodology to improve chatter free cutting conditions prediction. Int J Mach Tools Manuf 2013;72:16–24.
[71] Wang E, Wu B, Hu Y, Yang S, Cheng Y. Dynamic parameter identification of tool-spindle interface based on RCSA and particle swarm optimization. Shock Vib 2013;20(1):69–78.
[72] Mousavi S, Gagnol V, Ray P. Machining prediction of spindle-self-vibratory drilling head. J Mater Process Technol 2013;213(12):2119–25.
[73] Mehrpouya M, Graham E, Park SS. FRF based joint dynamics modeling and identification. Mech Syst Signal Process 2013;39(1-2):265–79.
[74] Xu C, Zhang J, Wu Z, Yu D, Feng P. Dynamic modeling and parameters identification of a spindle-holder taper joint. Int J Adv Manuf Technol 2013;67(5–8):1517–25.
[75] Albertelli P, Goletti M, Monno M. An improved receptance coupling substructure analysis to predict chatter free high speed cutting conditions. Procedia Cirp 2013;12:19–24.
[76] Law M, Altintas Y, Phani AS. Rapid evaluation and optimization of machine tools with position-dependent stability. Int J Mach Tools Manuf 2013;68:81–90.
[77] Law M, Rentzsch H, Ihlenfeldt S. Evaluating mobile machine tool dynamics by substructure synthesis. Advanced materials research vol. 1018. Trans Tech Publications; 2014. p. 373–80.
[78] Brecher C, Bäumler S, Daniels M. Prediction of dynamics of modified machine tool by experimental substructuring. Dynamics of coupled structures vol. 1. Cham: Springer; 2014. p. 297–305.
[79] Mancisidor I, Urkiola A, Barcena R, Munoa J, Dombovari Z, Zatarain M. Receptance coupling for tool point dynamic prediction by fixed boundaries approach. Int J Mach Tools Manuf 2014;78:18–29.
[80] Özşahin O, Özgüven HN, Budak E. Analytical modeling of asymmetric multi-segment rotor–bearing systems with Timoshenko beam model including gyroscopic moments. Comput Struct 2014;144:119–26.
[81] Wang L, Liu H, Yang L, Zhang J, Zhao W, Lu B. The effect of axis coupling on machine tool dynamics determined by tool deviation. Int J Mach Tools Manuf 2015;88:71–81.
[82] Özşahin O, Altintas Y. Prediction of frequency response function (FRF) of asymmetric tools from the analytical coupling of spindle and beam models of holder and tool. Int J Mach Tools Manuf 2015;92:31–40.
[83] Mehrpouya M, Graham E, Park SS. Identification of multiple joint dynamics using the inverse receptance coupling method. J Vib Control 2015;21(16):3431–49.
[84] Grossi N, Montevecchi F, Scippa A, Campatelli G. 3D finite element modeling of holder-tool assembly for stability prediction in milling. Procedia Cirp 2015;31:527–32.
[85] Xu C, Zhang J, Yu D, Wu Z, Feng P. Dynamics prediction of spindle system using joint models of spindle tool holder and bearings. Proceedings of the Institution of Mechanical Engineers, Part C: Journal of Mechanical Engineering Science 2015;229(17):3084–95.
[86] Özşahin O, Budak E, Özgüven HN. Identification of bearing dynamics under operational conditions for chatter stability prediction in high speed machining operations. Precis Eng 2015;42:53–65.

[87] Cao H, Xi S, Cheng W. Model updating of spindle systems based on the identification of joint dynamics. Shock Vib 2015.
[88] Yan R, Gao RX, Zhang L. In-process modal parameter identification for spindle health monitoring. Mechatronics 2015;31:42–9.
[89] Yang Y, Wan M, Ma YC, Zhang WH. An improved method for tool point dynamics analysis using a bi-distributed joint interface model. Int J Mech Sci 2016;105:239–52.
[90] Mehrpouya M, Sanati M, Park SS. Identification of joint dynamics in 3D structures through the inverse receptance coupling method. Int J Mech Sci 2016;105:135–45.
[91] Lu X, Jia Z, Wang H, Wang X, Si L, Gao L. Stability analysis for micro-milling nickel-based superalloy process. Int J Adv Manuf Technol 2016;86(9–12):2503–15.
[92] Liu H, Lu D, Zhang J, Zhao W. Receptance coupling of multi-subsystem connected via a wedge mechanism with application in the position-dependent dynamics of ballscrew drives. J Sound Vib 2016;376:166–81.
[93] Grossi N, Sallese L, Montevecchi F, Scippa A, Campatelli G. Speed-varying machine tool dynamics identification through chatter detection and receptance coupling. Procedia Cirp 2016;55:77–82.
[94] Grossi N, Scippa A, Montevecchi F, Campatelli G. A novel experimental-numerical approach to modeling machine tool dynamics for chatter stability prediction. J Adv Mech Des Syst Manuf 2016;10(2). JAMDSM0019–JAMDSM0019.
[95] Brecher C, Chavan P, Fey M, Daniels M. A modal parameter approach for receptance coupling of tools. Mm Sci J 2016:1032–4.
[96] Montevecchi F, Grossi N, Scippa A, Campatelli G. Improved RCSA technique for efficient tool-tip dynamics prediction. Precis Eng 2016;44:152–62.
[97] Matthias W, Özşahin O, Altintas Y, Denkena B. Receptance coupling based algorithm for the identification of contact parameters at holder–tool interface. Cirp J Manuf Sci Technol 2016;13:37–45.
[98] Zhao Y, Song X, Cai L, Liu Z, Cheng Q. Surface fractal topography-based contact stiffness determination of spindle-toolholder joint. Proc Inst Mech Eng Part C J Mech Eng Sci 2016;230(4):602–10.
[99] Kiran K, Satyanarayana H, Schmitz T. Compensation of frequency response function measurements by inverse RCSA. Int J Mach Tools Manuf 2017;121:96–100.
[100] Xu C, Feng P, Zhang J, Yu D, Wu Z. Milling stability prediction for flexible workpiece using dynamics of coupled machining system. Int J Adv Manuf Technol 2017;90(9–12):3217–27.
[101] Montevecchi F, Grossi N, Scippa A, Campatelli G. Two-points-based receptance coupling method for tool-tip dynamics prediction. Mach Sci Technol 2017;21(1):136–56.
[102] Xiaohong L, Zhenyuan J, Haixing Z, Shengqian L, Yixuan F, Liang SY. Tool point frequency response prediction for micromilling by receptance coupling substructure analysis. J Manuf Sci Eng 2017;139(7):071004.
[103] Qi B, Sun Y, Li Z. Tool point frequency response function prediction using RCSA based on Timoshenko beam model. Int J Adv Manuf Technol 2017;92(5-8):2787–99.
[104] Wang D, Wang X, Liu Z, Gao P, Ji Y, Löser M, et al. Surface location error prediction and stability analysis of micro-milling with variation of tool overhang length. Int J Adv Manuf Technol 2018:1–18.
[105] Junior MV, Baptista EA, Araki L, Smith S, Schmitz T. The role of tool presetting in milling stability uncertainty. Procedia Manuf 2018;26:164–72.
[106] Honeycutt A, Schmitz T. Receptance coupling model for variable dynamics in fixed-free thin rib machining. Procedia Manuf 2018;26:173–80.
[107] Jasiewicz M, Powałka B. Identification of a lathe spindle dynamics using extended inverse receptance coupling. J Dyn Syst Meas Control 2018;140(12):121015.
[108] Özşahin O. Determination of tool point FRF of micro tools under operational conditions using analytical methods. J Faculty of Eng Architec Gazi Univ 2018;33(2):529–39.
[109] Singh KK, Kulkarni SS, Kartik V, Singh R. A free interface component mode synthesis approach for determining the micro-end mill dynamics. J Micro Nanomanuf 2018;6(3):031005.
[110] Postel M, Özsahin O, Altintas Y. High speed tooltip FRF predictions of arbitrary tool-holder combinations based on operational spindle identification. Int J Mach Tools Manuf 2018;129:48–60.
[111] Ealo JA, Garitaonandia I, Fernandes MH, Hernandez-Vazquez JM, Muñoa J. A practical study of joints in three-dimensional Inverse Receptance Coupling Substructure Analysis method in a horizontal milling machine. Int J Mach Tools Manuf 2018;128:41–51.
[112] Li Z, Wang Z, Shi X, Li W. RCSA-based prediction of chatter stability for milling process with large axial depth of cut. Int J Adv Manuf Technol 2018;96(1-4):833–43.
[113] Shaik JH, Ramakotaiah K, Srinivas J. Frequency response studies using receptance coupling approach in high speed spindles. J Inst Eng 2018:1–12.
[114] Jasiewicz M, Powałka B. Prediction of turning stability using receptance coupling. AIP Conference Proceedings 2018;Vol. 1922. No. 1, p. 100005.
[115] Ji Y, Bi Q, Zhang S, Wang Y. A new receptance coupling substructure analysis methodology to predict tool tip dynamics. Int J Mach Tools Manuf 2018;126:18–26.
[116] Tunc LT. Prediction of tool tip dynamics for generalized milling cutters using the 3D model of the tool body. Int J Adv Manuf Technol 2018;95(5-8):1891–909.
[117] Liao J, Yu D, Zhang J, Feng P, Wu Z. An efficient experimental approach to identify tool point FRF by improved receptance coupling technique. Int J Adv Manuf Technol 2018;94(1-4):1451–60.
[118] Bishop RED, Johnson DC. The mechanics of vibration. Cambridge: Cambridge University Press; 1960.